3. Materials and apparatus

In this study, we used Fujinomori soil (sample 1), three types of glass particles with uniform sizes (Catalysts and Chemicals Ind. Co., Ltd.: d = 9.7 μm (sample 2), d = 5.3 μm (sample 3), d = 2.2 μm (sample 4) and mixture of the glass particles (sample 5). All water that we used was preliminary distilled, deionized, and degassed.

The sample 1 was actual soil and well-known for its high frost susceptibility. The particles in the samples 2-4 were spherical with roughly the same diameters and their surface had nano-pores with a uniform diameter (figures 6 and 7). The sample 5 was prepared by mixing the samples 2-4 and two other kinds of glass particles with uniform diameters (Nippon Rikagau Kikai Co., Ltd.: d = 50 μm and d = 200 μm). In the case of the sample 5, the particle size distribution was arranged to the distribution of the sample 1. The sample 1 was prepared for observing actual ice lensing in natural soils and the samples 2-4 were for observing ideal ice lensing to make model. The sample 5 was prepared for comparing the phenomena between actual soil and ideal porous media and for verifying influence of the uniformity of particles on a model that will be shown in chapter 7.

3.1 Characteristics of samples and grain-size distribution

Table 1 lists some characteristics of the samples 1-5. Some values for the sample 1 were quoted from Takeda (1988). The samples 2-4 consisted of Vycor glass particles, which formed a fine powder.

Table 1. Characteristics of the samples 1-5

Sample		Sample 1 Fujinomori	Sample 2 Glass	Sample 3 Glass	Sample 4 Glass	Sample 5 Mixture
Gravel	(2.00mm~)%	0	0.0	0.0	0.0	0
Sand	(2.00~0.074mm)%	15	0.0	0.0	0.0	15
Silt	(0.074~0.005mm)%	61	97.3	45.9	12.6	60
Clay	(~0.005mm)%	24	2.78	54.1	87.4	25
Mineral components		Quartz, Feldspar (little), Kaolin, Mica, Montmorillonite, etc. (very little)	SiO_2 (99.6%), Na_2O (little) etc. (very little)	SiO_2 (99.0%), Na_2O(little) etc. (very little)	SiO_2 (99.4%), Na_2O(little) Etc. (very little)	SiO_2 (99.0%), etc. (little)
Mean diameter	μm	-	9.7	5.3	2.2	-
Specific gravity	gcm^{-3}	2.61	2.12	2.13	2.12	-
Specific surface area	m^2g^{-1}	24.5	150.5	146.4	128.6	-
Liquid limit		45.3	79.0	79.0	79.0	34.1
Plastic limit		46.5	79.0	79.0	79.0	34.1
Dry density	$g\ m^{-3}$	1.18	0.79	0.82	0.85	0.88
Porosity	n %	55.0	-	-	-	-
Hydraulic conductivity	K cm s^{-1}	2.22×10^{7}	5.85×10^{-6}	3.00×10^{-6}>	3.00×10^{-6}>	-
Thermal conductivity	cal $cm^{-1}s^{-1}°C^{-1}$	2.68×10^{-3}	-	-	-	-
pH		-	6.8	7.0	6.8	7.0

Figure 6 shows grain size accumulation curves for the samples. The sample 1 was mainly consisting of silt. The grain size of the sample 1 gradually distributed from 0.3 mm to clay size. The mean particle diameters of samples 2 and 4 corresponded to silt and clay, respectively. The particle diameter of sample 3 was just between the samples 2 and 4. The coefficient of uniformity U_c of the samples 2 and 3 were 1.81 and 3.18 and the coefficient of curvature U_c' were 1.02 and 1.19, respectively. Although, the distribution of sample 4 was not so obvious because of the lack of measurement under the range of a few micrometers, it was found that the particle sizes of samples 2 and 3 were very uniform. The particle size distribution of the sample 5 imitated the distribution of sample 1. Figure 6 indicates that the sample 5 had almost same particle distribution as the sample 1.

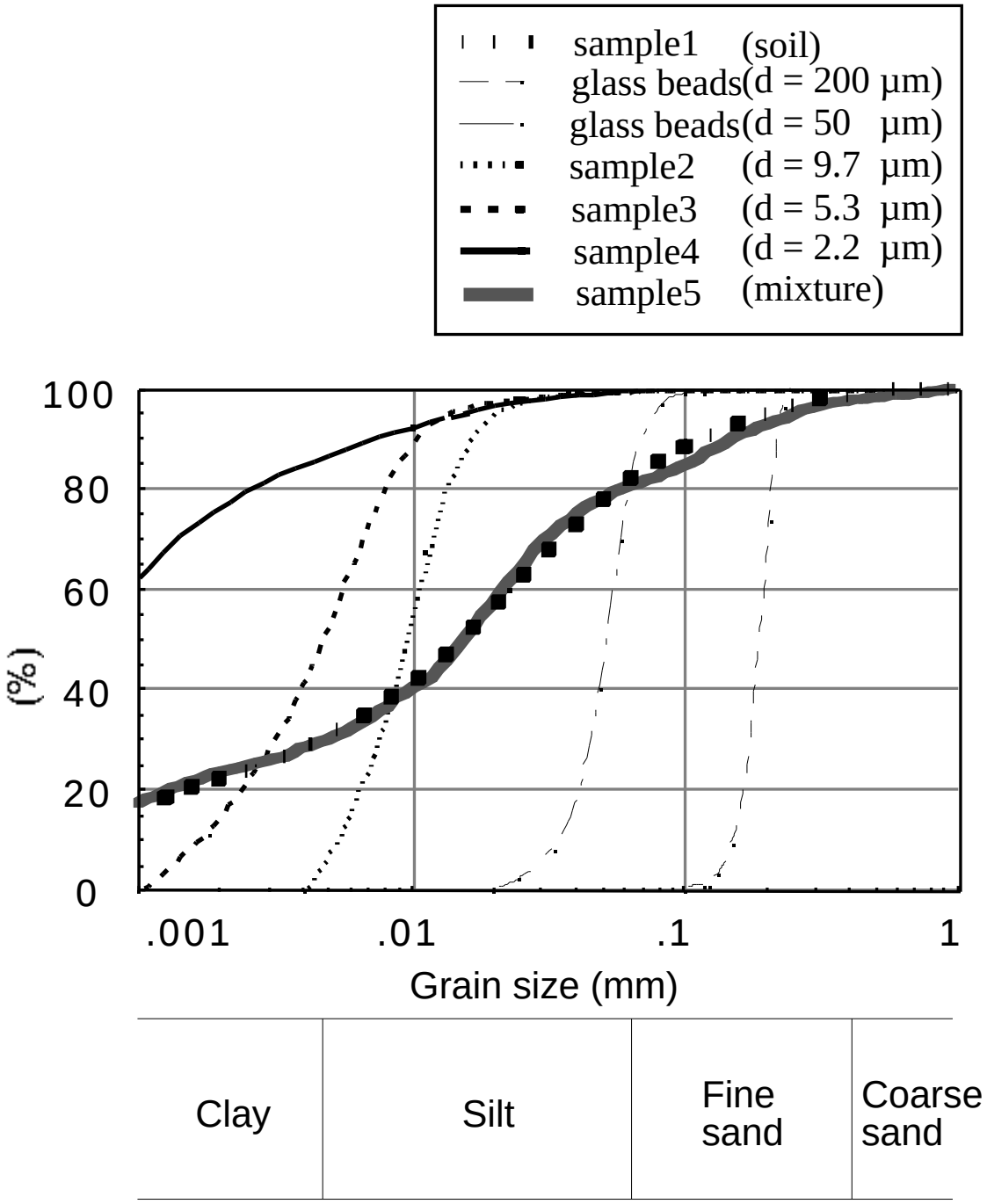

Fig. 6. Grain size accumulation curves for the samples.

3.2 Surface conditions

The surfaces of sample particles were observed by electron microscope. Figures 7a-d show the electron micrographs of the samples 1-4. The samples were coated with thin film of vacuums evaporated gold since a sample must have some electric conductivity for observation by electron microscope. Then, the surface was observed with resolution of until 50000 but the surface under the film could not observed. In the micrographs with resolution of 50000, the thin film of gold was shown as a plane with many cracks. Such cracks distributed widely throughout the surface shown in the micrographs. In the figure 7a (Sample 1), plate-like particles with diameter of dozens micrometer and a number of micro particles with diameter of a few micrometer were observed. In the figure 7b (Sample 2), spherical particles with diameters from 3 to 20 micrometers were observed. The particles had many granular matters less than 0.3 micrometer on the surface. In the figure 7c (Sample 3), spherical particles with diameters from 1 to 15 micrometers were observed. The aspects were similar to the sample 2. The particle surface shown in the figure 7c also had granular matters less than 0.3 micrometer. In the figure 7d (Sample 4), spherical particles with diameters from 0.1 to 6 micrometers were observed. Some of these particles gathered and aggregated. The surface also had some granular matters

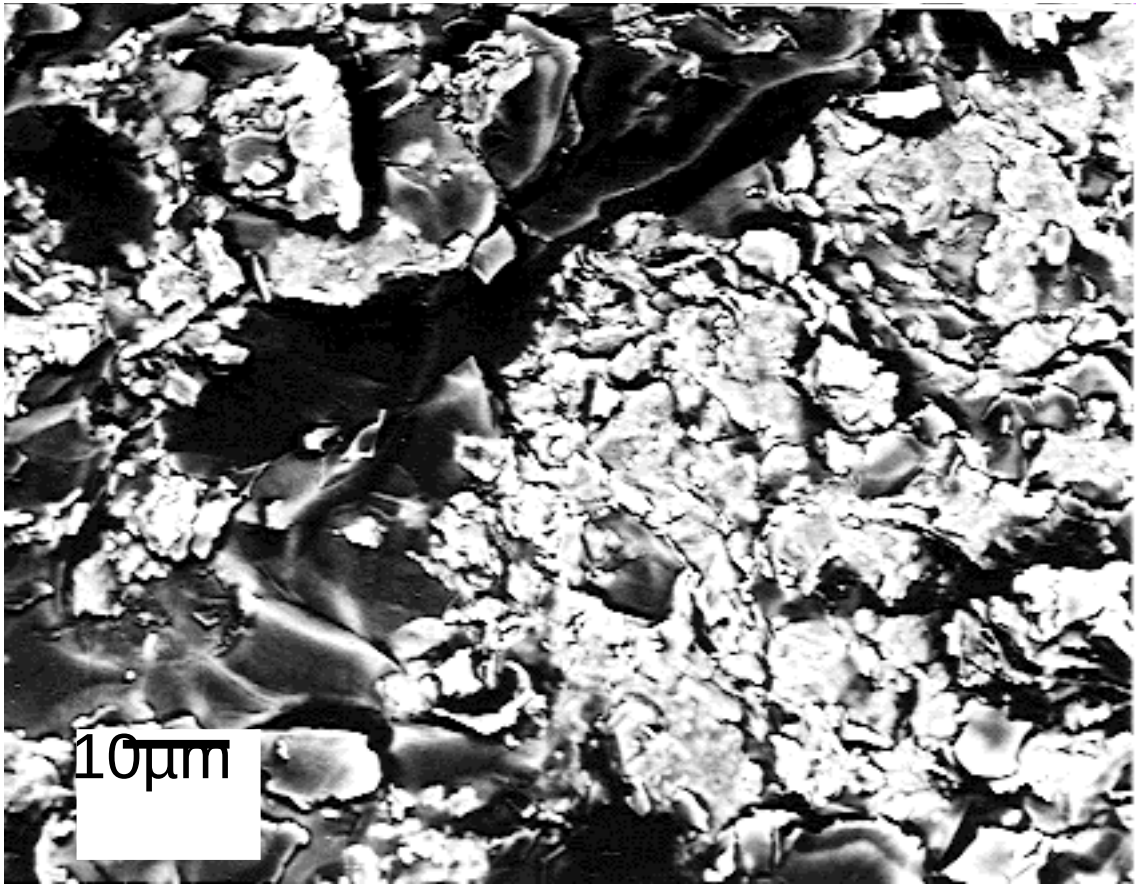

Fig. 7. (a) Electron micrograph of sample 1 (Fujinomori soil: × 1000).

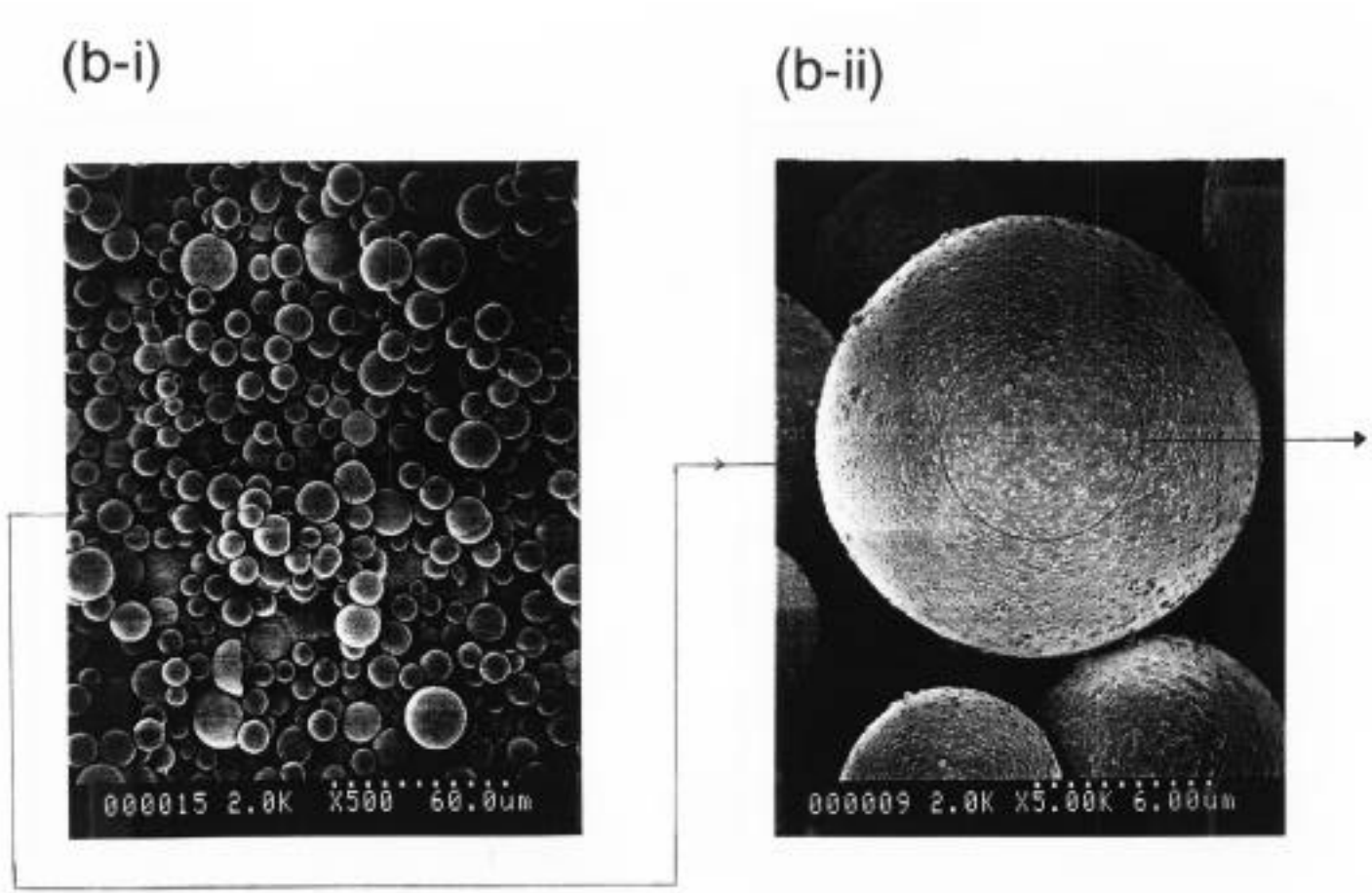

Fig. 7. (b) Electron micrograph of sample 2. (i) × 500, (ii) × 5000.

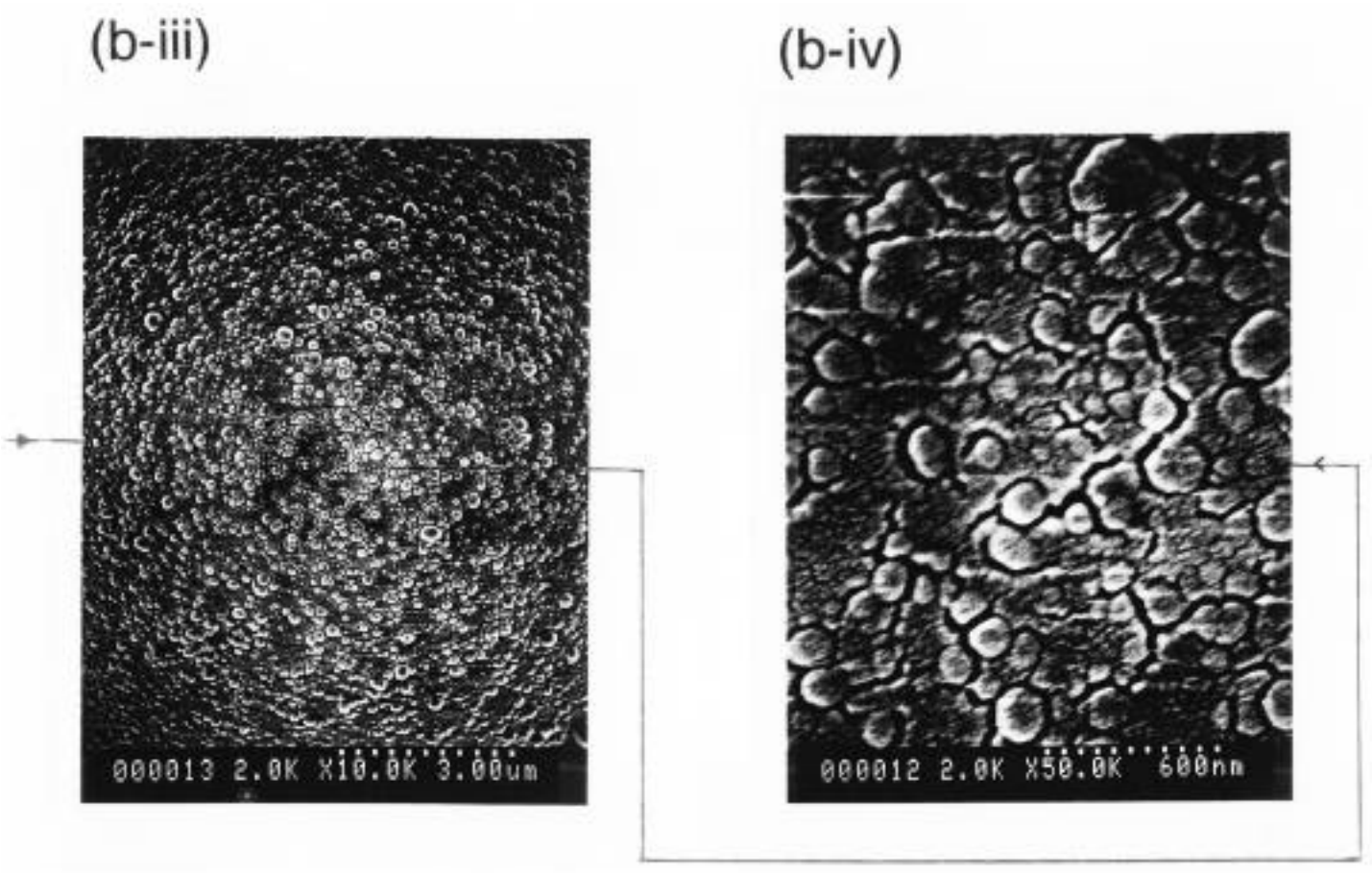

Fig. 7. (b) Electron micrograph of sample 2. (iii) × 10000, (ii) × 50000.

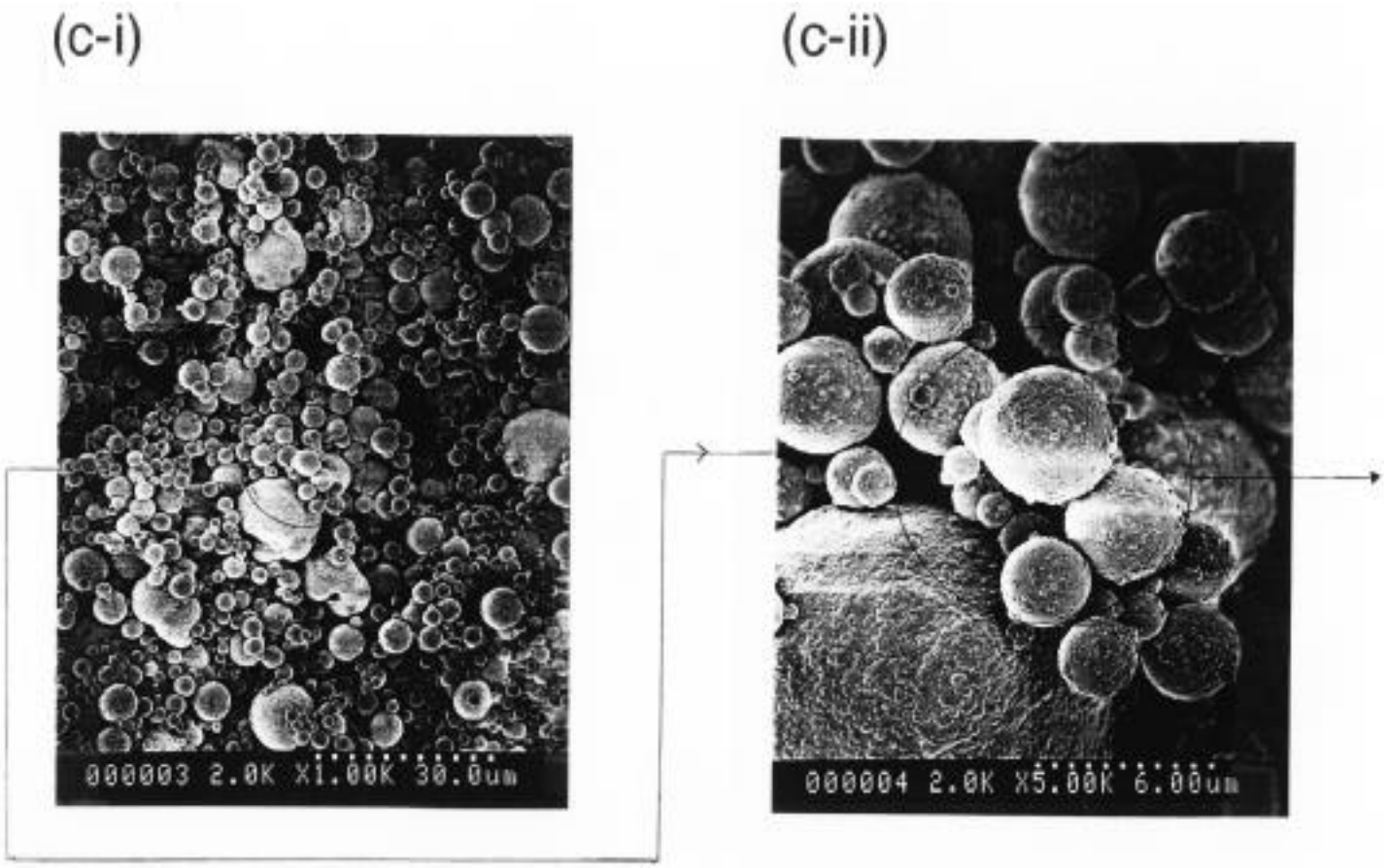

Fig. 7. (c) Electron micrograph of sample 3. (i) × 500, (ii) × 5000.

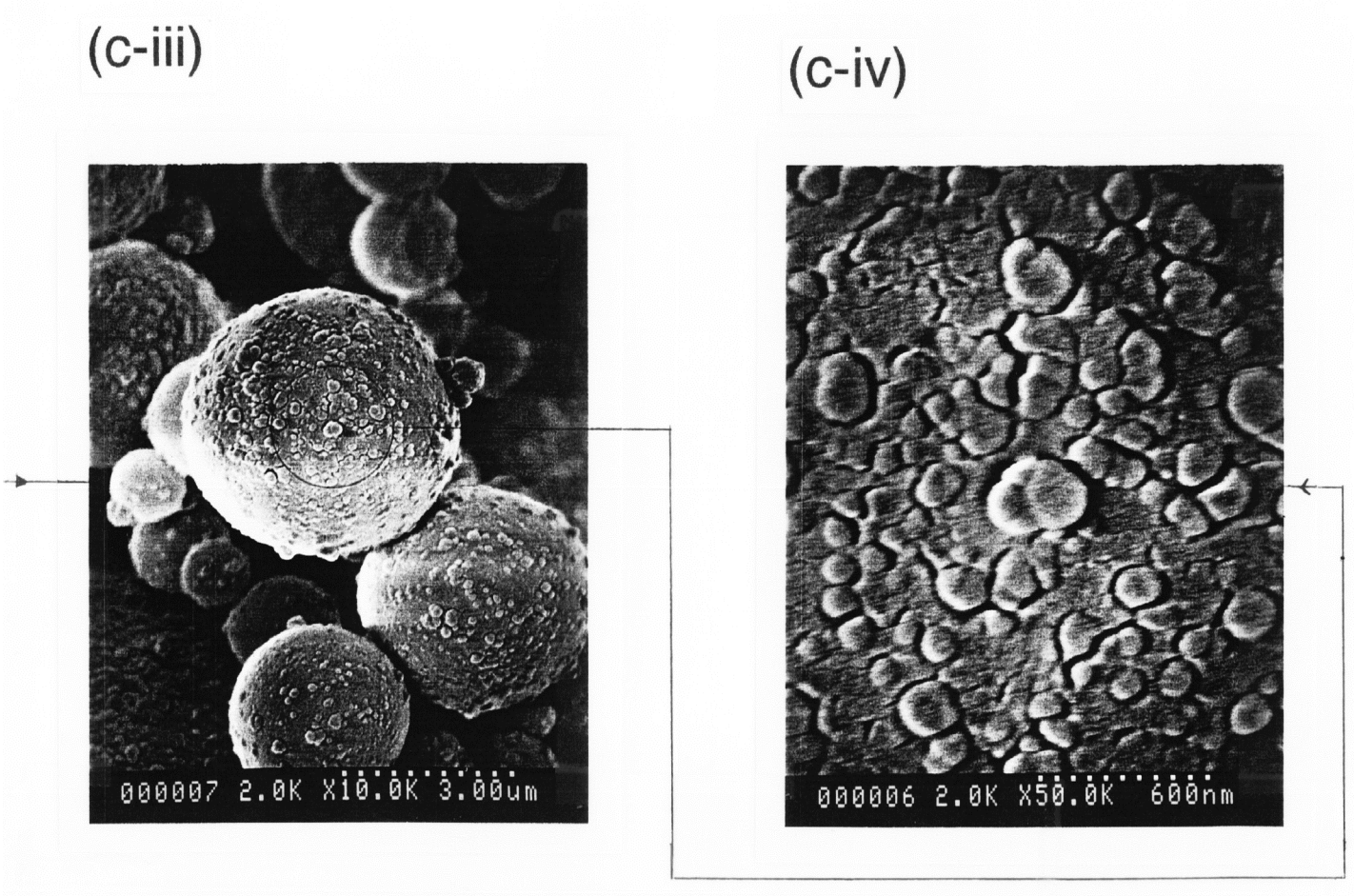

Fig. 7. (c) Electron micrograph of sample 3. (iii) × 10000, (ii) × 50000.

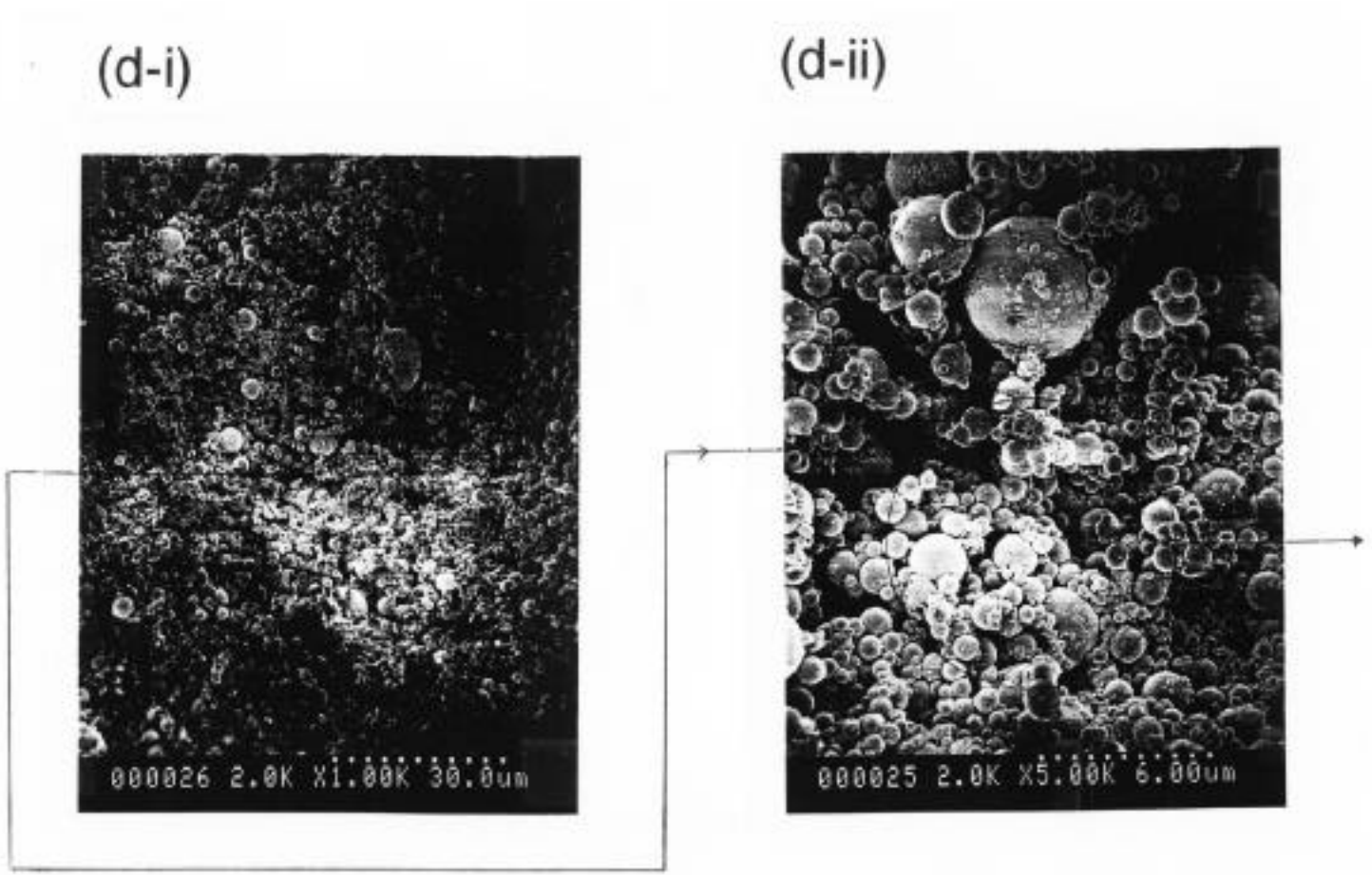

Fig. 7. (d) Electron micrograph of sample 4. (i) × 500, (ii) × 5000.

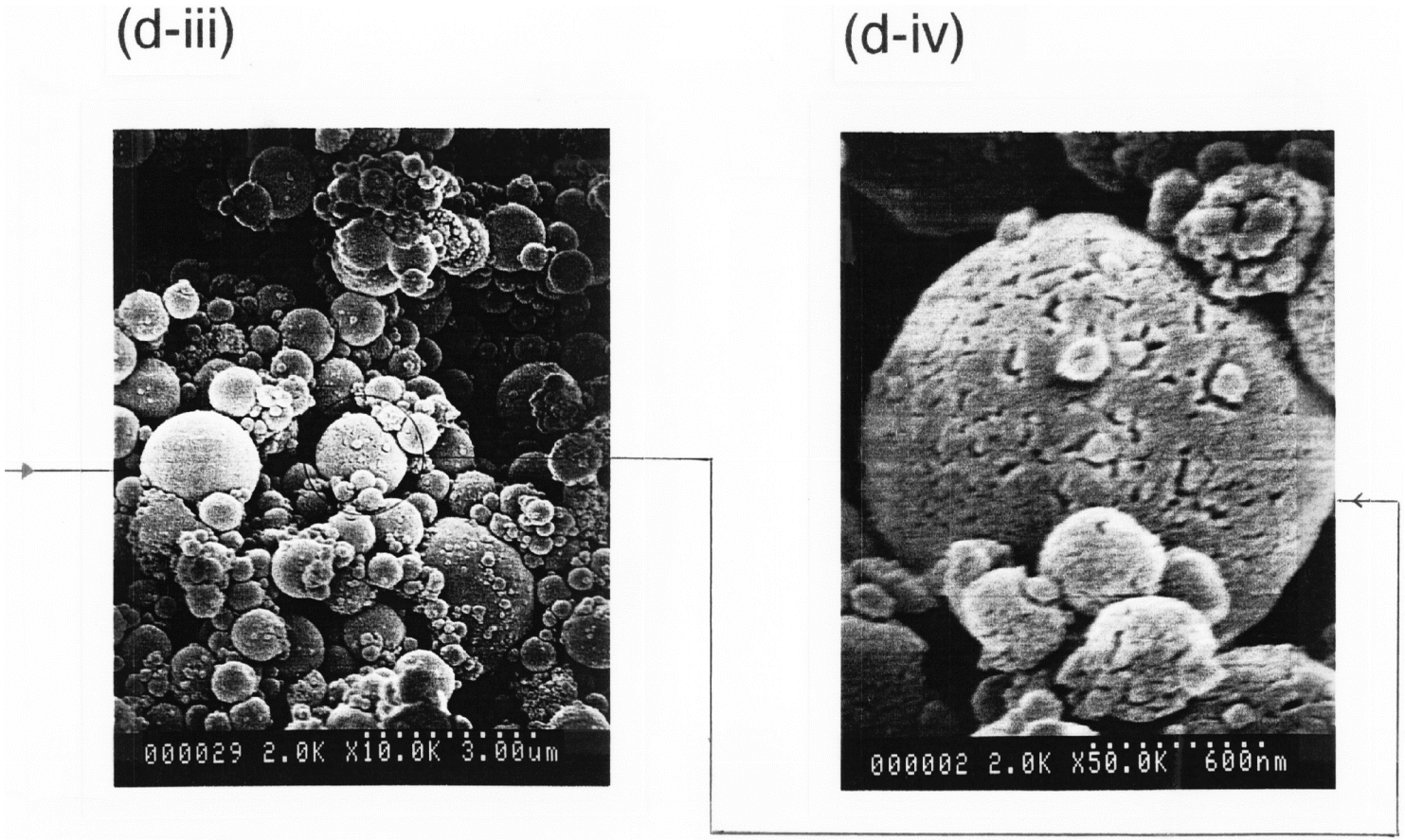

Fig. 7. (c) Electron micrograph of sample 3. (iii) × 10000, (ii) × 50000.

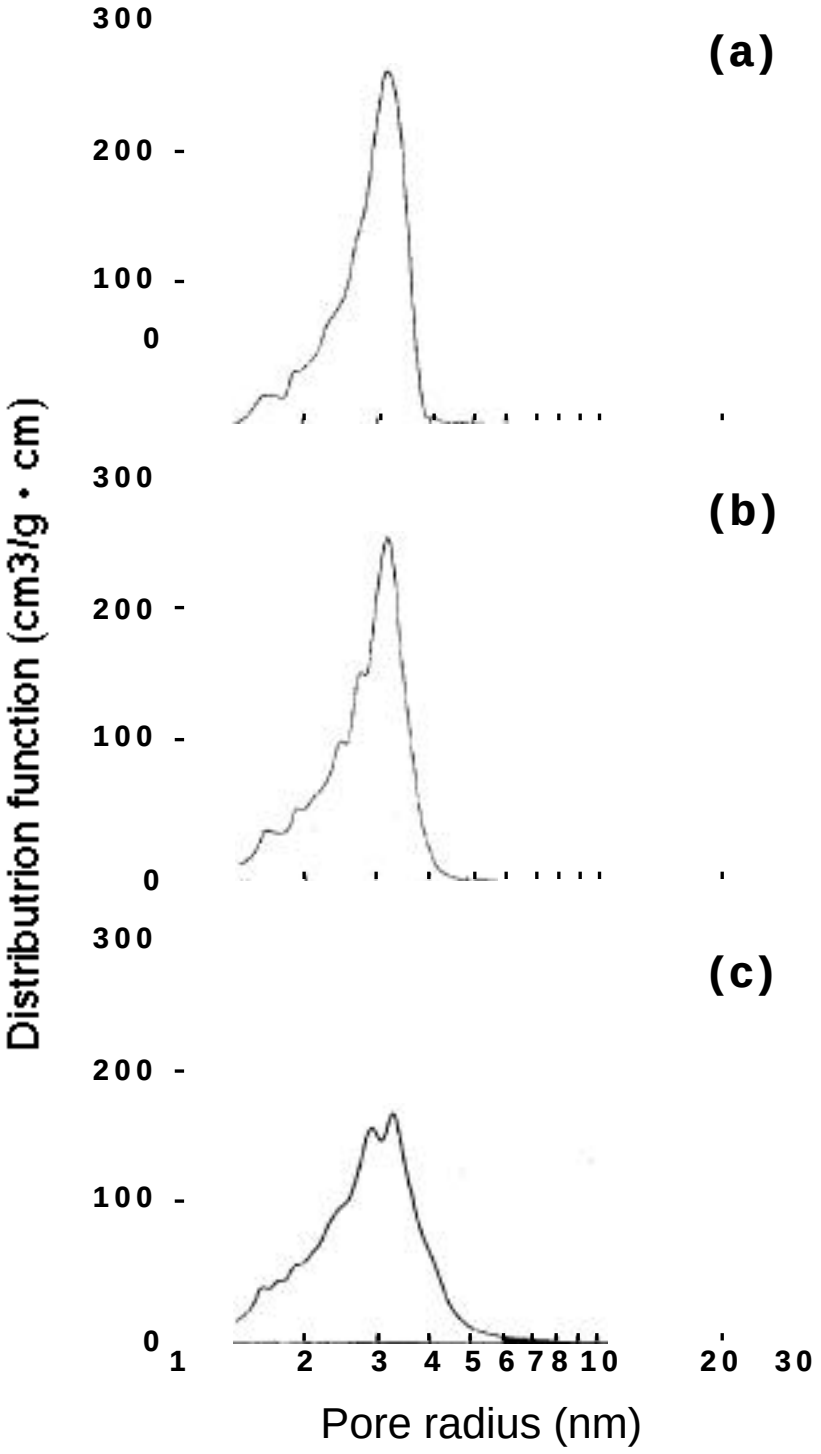

Fig. 8. Distribution curves of nano pores of the samples 2-4 obtained by the nitrogen adsorption method. (a) Sample 2 (d = 9.7 μm), (b) Sample 3 (d = 5.3 μm), (c) Sample 4 (d = 2.2 μm). Each curve has strong peak at 3.3 nm.

3.3 Specific surface area and distribution of pores

The specific surface area and distribution of nano-pores were determined by nitrogen adsorption method. Nitrogen gas tends to adsorb to a surface as monolayer. The method consists of the measurement of the amount of nitrogen gas adsorbed and subsequent calibration of this amount with the specific surface area. Table 1 shows the specific surface area of the samples measured by using auto gas adsorption apparatus (Nihon Bell Co. Ltd.: BEL SORP36). A sample that has higher specific surface area may have more amount of unfrozen water during freezing. Each specific surface area of the samples 2-4 was over 120 (m^2/g), which was greater than the value of montmorillonite (80 m^2/g). These high specific surface areas imply that the samples might have a lot of unfrozen water at subzero temperature. Figure 8 shows distribution curves of nano pores of the samples 2-4 obtained by the nitrogen adsorption method. Each curve had strong peak at 3.3 nm. The high specific surface areas of samples will come from the presence of nano pores.

3.4 Unfrozen water content

3.4.1 NMR methods

The unfrozen water content can be defined as ratio of liquid water (g) to sample (100 g). Since all the water melt, the content of unfrozen sample remains constant value, which corresponds to normal water content (wt%). The unfrozen water content was measured using pulsed NMR technique. A proton bears a slight magnetic moment originating from its spin, and acts as magnet that tends to align along a fixed external magnetic field. The magnetic moment orients when pulse is applied to a sample set in fixed magnetic field and it returns to the initial direction when the pulse is eliminated. An NMR measured a change in magnetic field arising at the time as voltage decay. The voltage decay curve is called a free-induction decay (FID). FID

peak value proportional to the number of protons of water and ice in the sample. The FID signal resulting from ice, however, decreases much rapider than the signal from liquid water. Therefor, we can estimate amount of liquid water in a sample from the FID.

3.4.2 Test procedure

We used a pulsed NMR instrument PRAXIS-2 shown in figure 9 and photograph 3. The applied magnetic filed was 2.5 kG, the radio frequency was 10.7 MHz and the pulse width was 12 μm. Samples were prepared by placing soil or glass particles in a desiccator with water, evacuating the desiccator, allowing a few days for the solid-vapor equilibrium to be established, adding liquid water, and allowing the system to equilibrate for one day. The initial water content of the sample 1 was 50% and of the samples 2-4 were 80 %, respectively. The prepared samples were compacted in a Teflon tube with diameter of 25 mm for NMR measurements and sealed off with rubber stopper to prevent water evaporation. The samples were first frozen at –40 ˚C. Then, series of unfrozen water content of the samples were measured during the sample thawing from –40 ˚C to 10 ˚C.

3.4.3 Unfrozen water content

Figure 10 shows unfrozen water content in the frozen samples measured using the NMR technique. The unfrozen water content in each sample decreased steeply near 0 ˚C. The unfrozen water content of the sample 1 almost reached 0 % at –20 ˚C. The samples 2-4 had 5 % or more unfrozen water even under –30 ˚C. The samples 2-4 had similar water content curves. Unfrozen water presence exists on the surface of particles. Therefor, the amount of unfrozen water of a sample will be proportional to its surface area and highly depend on the surface condition. Since the samples 2-4 had

similar nano-pore distribution and similar specific surface area in spite of different diameters, the samples would have similar curves of unfrozen water content shown in the figure 10. Large amount of unfrozen water of the samples also would come from their high specific surface area and the nano-pores.

3.4.4 Effect of solute on unfrozen water content

Unfrozen water content of the sample 1 saturated with solution instead of distilled water was also measured. We can find the effect of solute on the soil freezing from the measurements of the unfrozen water. The solutes we used were NaCl, KCl and $MgCl_2$. The solutes were mixed with distilled water and 9 kinds of solutions (10, 3, 2, 1, 0.5, 0.1, 0.05, 0.01, 0 wt%) were prepared. Figures 11a-c show the unfrozen water curves of samples 1 saturated with NaCl, KCl and $MgCl_2$ solutions, respectively. In the figures, FJ indicates the sample 1 saturated with distilled water, and 10 % and 1 % indicate the samples saturated with the concentration of solutes, respectively. The unfrozen water contents were maintained the initial water content a few degrees lower than 0 ˚C because of the depression of freezing point induced by the solutes. The sample, which had high concentration of solute, had large amount of unfrozen water. Such dependence of solute on the unfrozen water amount was shown in other samples saturated with different solutes (Watanabe and Mizoguchi, 1997).

Photograph 3. A pulsed NMR instrument PRAXIS-2.

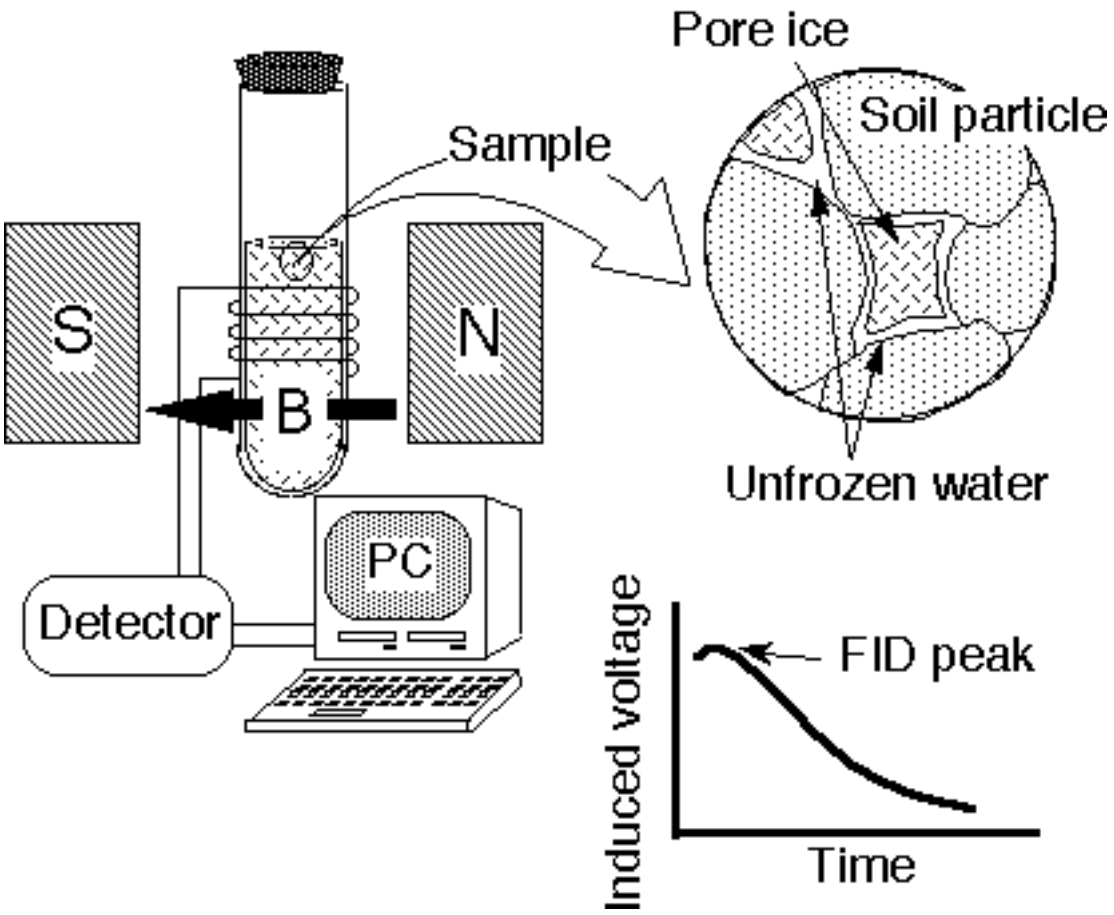

Fig. 9. Schematic diagram of NMR setup, a sample and a resulting NMR signal.

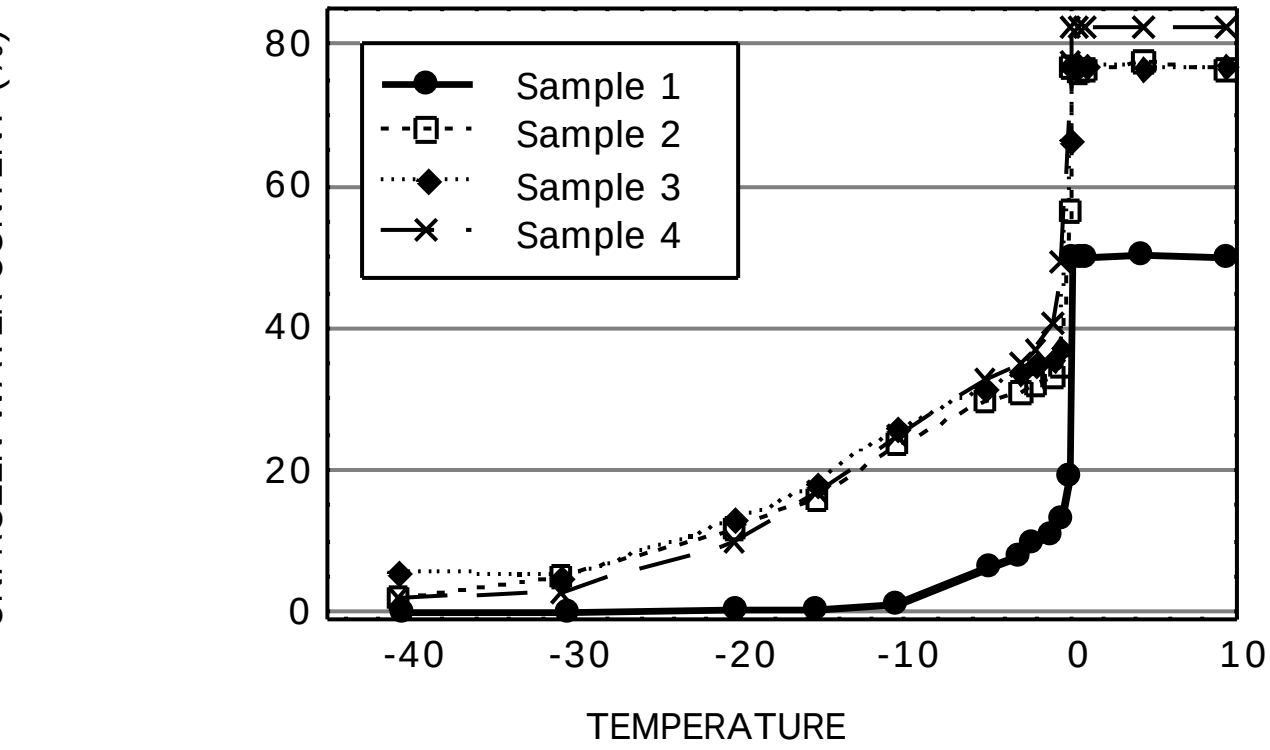

Fig. 10. Unfrozen water content in the frozen samples measured using the NMR technique.

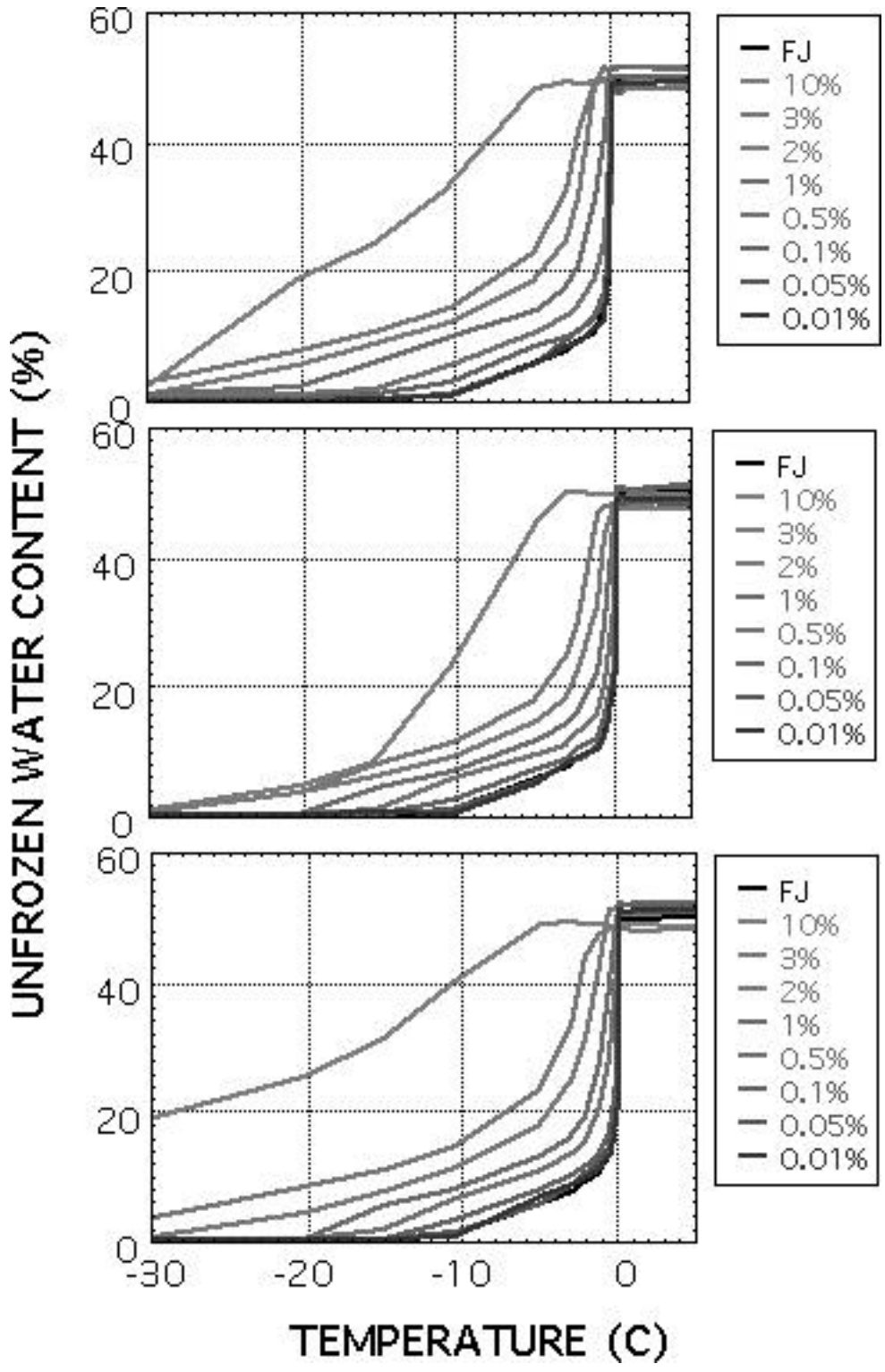

Fig. 11. Unfrozen water curves of samples 1 saturated with NaCl, KCl and $MgCl_2$ solutions.

3.5 Unidirectional freezing apparatus

In this study, the sample was frozen using the unidirectional freezing apparatus shown in photograph 4, which is basically the same as that designed by Uhlmann *et al.* (1964), Uhlmann and Jackson (1985), Köber *et al.* (1992) and Nagashima and Furukawa (1997). The advances of using the apparatus are that we can easily control temperature gradient and freezing rate for a sample and that we can observe near the crystal growth surface continuously, directly and microscopically.

Schematic diagrams of the apparatus are shown in figure 12. The sample prepared was set into the sample cell. The sample cell was placed in a Teflon cell holder indicated by a star mark;☆. Opposite ends of the cell were held at different temperatures, T_H and T_L, by using two copper blocks kept at constant temperatures by Peltier thermoelements. The thermoelements were controlled by a computer at each 6-second. This established a temperature gradient α in the sample cell. The left side of the figure is warmer and the right side is colder.

The cell holder was moved toward the cold side at a constant rate from 0 to 40 μm/sec by a computer controlled pulse motor. When the cell was moved with constant rate V_s, the sample was cooled with keeping established temperature gradient α. The advancing rate of isotherms in the sample V_f corresponded to the constant rate of the sample moving V_s ($V_f = -V_s$: figure 13). In this time, the freezing front in the sample did not move against the observation filed of microscope since the sample was moved relative to the freezing. Consequently, continuous direct observation was available with a microscope.

Photograph 4. Unidirectional freezing apparatus.

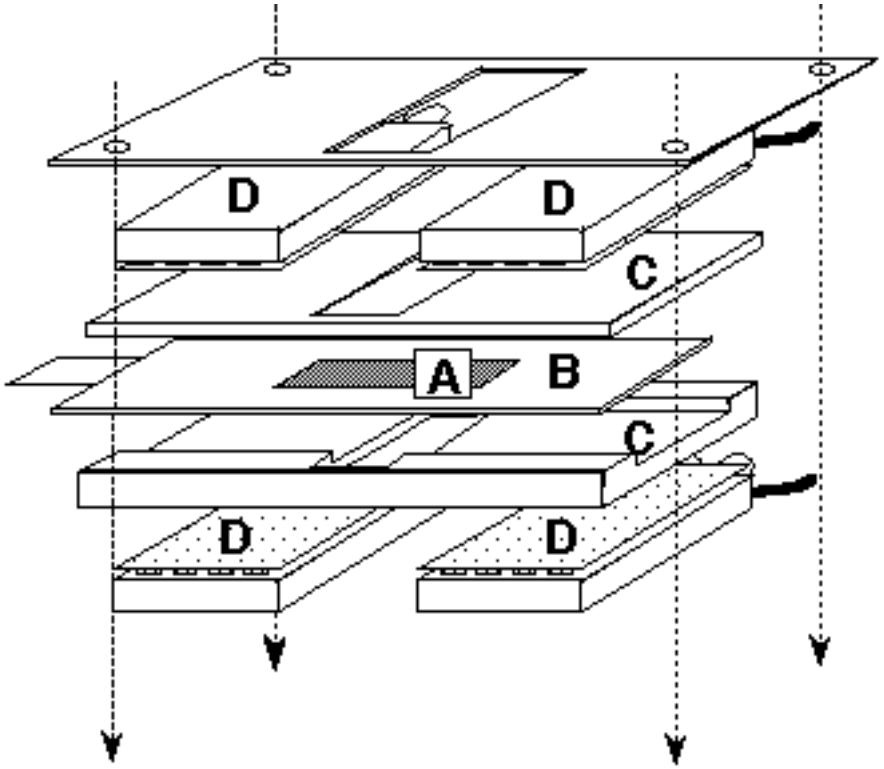

Fig. 12a. Schematic diagram of unidirectional freezing apparatus (freezing portion).
A: sample cell, B: teflon holder, C: copper block, D: thermoelement

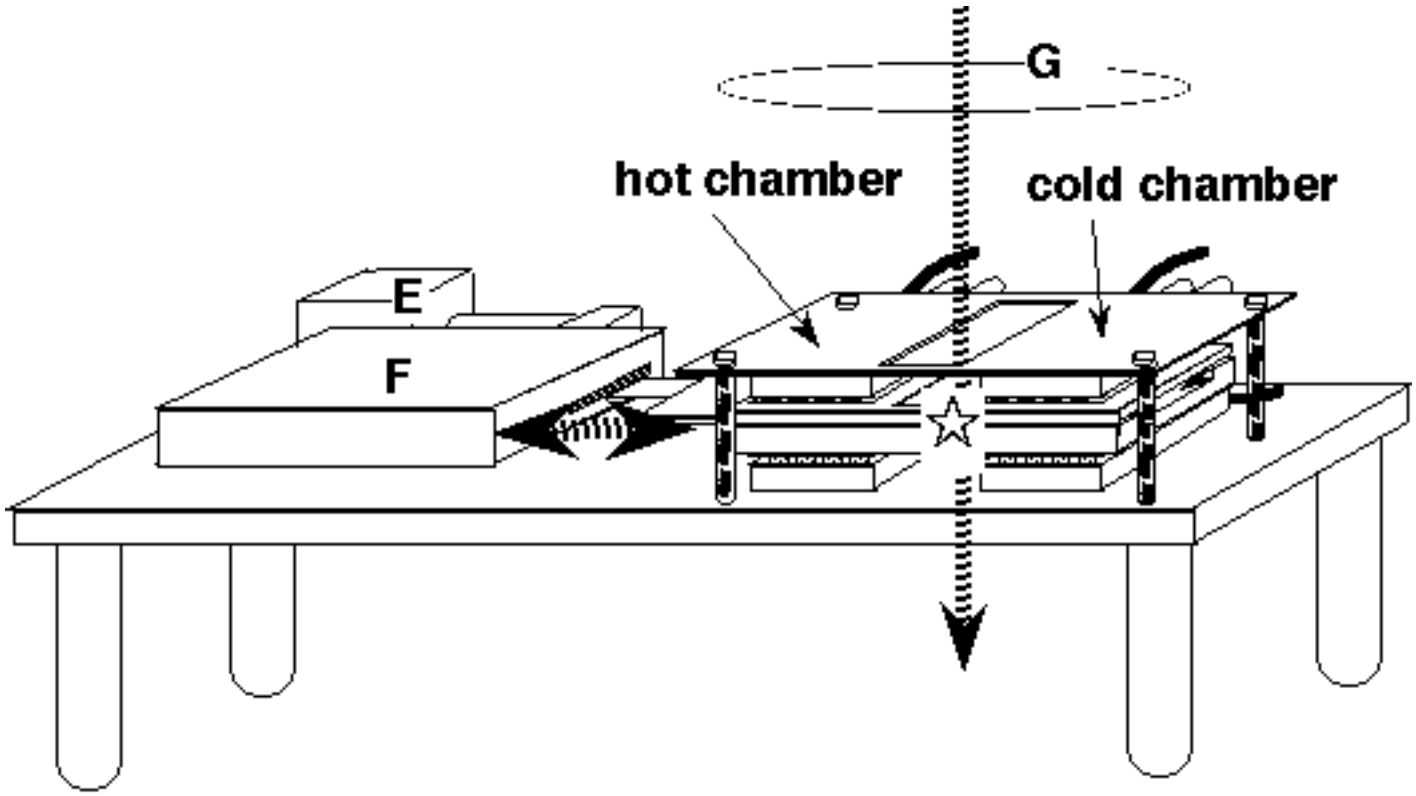

Fig. 12b. Schematic diagram of unidirectional freezing apparatus.
E: pulse motor, F: translational stage, G: microscope.

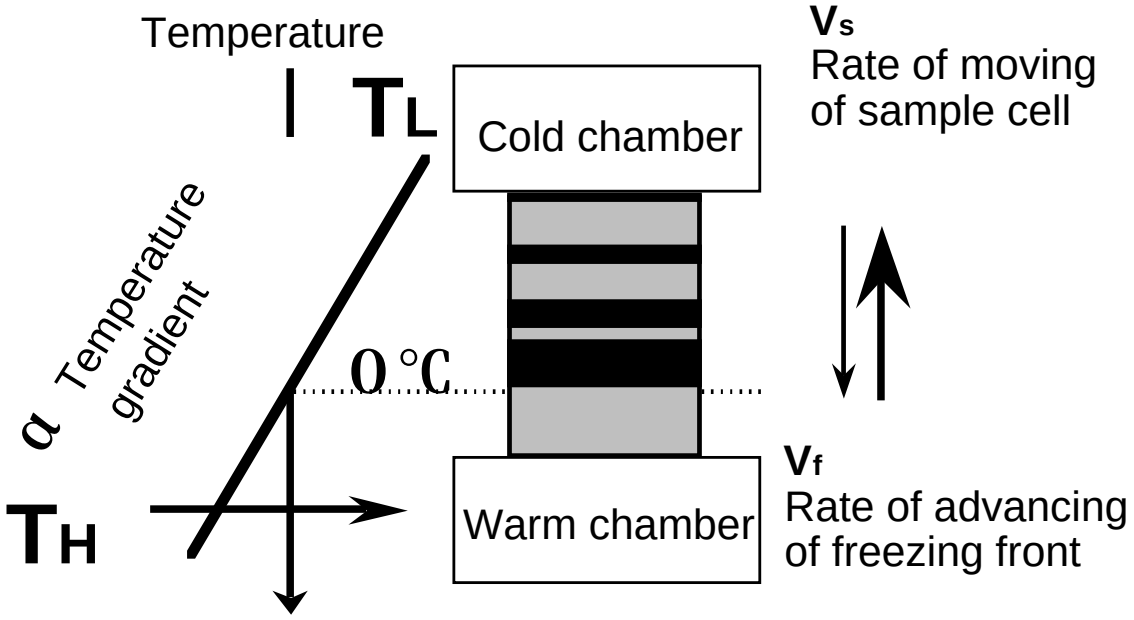

Fig. 13. Schematic diagram of temperature gradient and freezing rate given to the sample on the unidirectional freezing apparatus.

The temperature of each chamber is controlled by thermoelement. Then a constant temperature gradient, α, is maintained in the sample. The sample cell is pushed toward the cold chamber at a constant speed, V_s by a computer-controlled pulse motor. When V_s is zero, the isotherms moved immediately after lowering the temperature. When V_s is not zero, the freezing rate of advancing of freezing front, V_f is equal to the rate of moving of sample cell, V_s.